Catalysis Letters Vol. 101, Nos. 1–2, May 2005 (© 2005)
DOI: 10.1007/s10562-005-3758-0

Branching of the intermediate N_2O decomposition in a steady-state NO + CO + O_2 reaction on Pd(110); an angle-resolved desorption study

Y. -S. Ma, I. I. Rzeznicka, and T. Matsushima*

Catalysis Research Center, Hokkaido University, Sapporo, 001-0021, Japan

Received 19 October 2004; accepted 10 January 2005

The branching of the intermediate N_2O decomposition vs. the desorption was studied in a steady-state NO + CO + O_2 reaction on Pd(110). Three surface-nitrogen removal processes, i.e., $N_2O(a) \rightarrow N_2(g) + O(a)$, $N_2O(a) \rightarrow N_2O(g)$ and $2N(a) \rightarrow N_2(g)$, are operative. Only about 20% of $N_2O(a)$ was desorbed without decomposition for a (NO:CO = 1:1) mixture. The fraction increased steeply with increasing surface oxygen.

KEY WORDS: nitrous oxide; nitrogen oxide; nitrogen; decomposition; palladium; angular distribution.

1. Introduction

The NO reduction by CO, H_2 and hydrocarbon on rhodium and palladium surfaces has received much attention because of its importance in controlling automobile exhaust gas. In this catalytic reduction, N_2O is concomitantly produced as one of the undesired byproducts [1]. This species is not only a harmful byproduct with a significant greenhouse effect but also the key intermediate for controlling the selectivity to N_2 because its decomposition shares the main pathway [2,3]. However, knowledge of this pathway is limited especially in the presence of gaseous oxygen, i.e., under lean-burn conditions [4]. This paper delivers the first analysis of three surface-nitrogen removal processes, i.e., (i) the decomposition of the intermediate, $NO(a) + N(a) \rightarrow N_2O(a) \rightarrow N_2(g) + O(a)$, (ii) N_2O desorption without decomposition and (iii) the associative desorption of nitrogen atoms, $2N(a) \rightarrow N_2(g)$, in a steady-state NO + CO + O_2 reaction on Pd(110). Only about 20% of the formed intermediate $N_2O(a)$ was desorbed without decomposition when the surface was rather deficient in O(a). The fraction increased steeply with increasing surface oxygen. The contribution of process (iii) relatively increased at high surface temperatures.

The ordinary kinetic study at the steady-state NO reduction is not informative for surface-nitrogen removal processes because of the presence of several fast pathways after the slow NO dissociation [5]. On the other hand, the angular and velocity distributions of desorbing products can provide information of the desorption process whenever any step becomes rate-determining since these distributions do not involve the reaction rate directly [2,6]. Furthermore, process (i) emits N_2 in an inclined way, process (ii) yields a broad N_2O distribution, and process (iii) sharply emits N_2 along the surface normal [7,8].

Those distributions were frequently analyzed in the course of the catalyzed NO reduction with several relaxation methods to avoid the well-known large N_2 formation on the reaction chamber wall [8–12]. Steady-state conditions, however, cannot be established for the reaction. In the present work, angle-resolved (AR) product desorption was successfully analyzed for the steady-state NO + CO + O_2 reaction by using a gas doser with a fine orifice.

2. Experiments

The experiments were performed in an ultra-high vacuum apparatus composed of three chambers [13]. The principle behind the apparatus is shown in Figure 1. The reaction chamber was equipped with reverse-view low-energy electron diffraction (LEED) and X-ray photo-electron spectroscopy (XPS) optics, a quadrupole mass spectrometer (QMS) and an Ar^+ gun. The chopper house contained a cross-correlation chopper and an analyzer with another QMS for AR and time-of-flight (TOF) analyses [13]. The distance from the ionizer to the chopper blade was 377 mm and the time resolution was selected at 20 μs. A mixture of ^{15}NO and ^{12}CO (or ^{14}NO and ^{13}CO) was introduced to the surface through a doser with a fine orifice while O_2 was backfilled. Hereafter, the isotopes of ^{13}C and ^{15}N are simply designated as C and N in the text. The steady-state formation of

* To whom correspondence should be addressed.
E-mail: tatmatsu@cat.hokudai.ac.jp

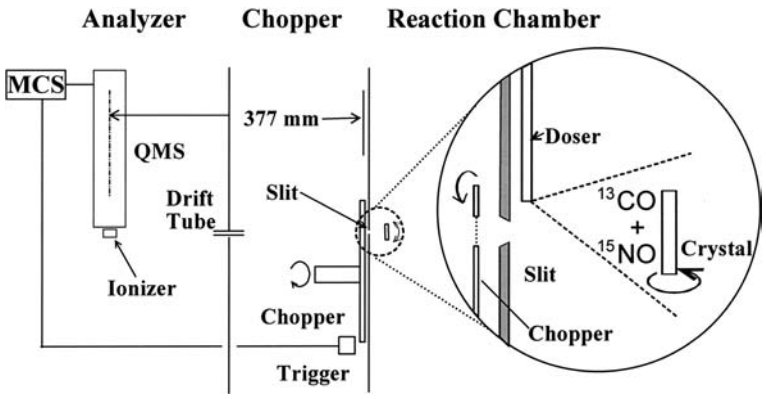

Figure 1. Apparatus for angle-resolved product desorption combined with cross-correlation time-of-flight techniques. The insert shows the structure around a sample crystal and a gas doser. QMS (quadrupole mass spectrometer); MCS (multichannel scalar); trigger (photocell and light-emitting diode). The chopper house is pumped at about 7 m^3 s^{-1}.

N_2, CO_2 and N_2O was monitored in both angle-integrated (AI) and AR forms. The AI signal was determined by QMS in the reaction chamber as the difference in the signal between the desired surface temperature (T_S) and room temperature. On the other hand, the AR signal was obtained by QMS in the analyzer as the difference between the signal at the desired angle and the signal when the crystal was away from the line-of-sight position. The desorption angle (θ; polar angle) was scanned in the normally directed plane along the [001] direction [2]. The fragmentation of N_2O in both QMS's was corrected.

3. Results

3.1. NO + CO reaction

The steady-state NO + CO reaction became observable above 500 K. It showed a maximum and decreased above about 550 K. In Figure 2a, the AR CO_2 signal at $\theta = 0°$ is shown vs. T_S since it showed very similar T_S dependence to that of the overall reaction rate because its desorption always collimated along the surface normal and the byproduct N_2O formation was much less (below 20%) than that of CO_2. Only the (1×1) pattern was observed in LEED measurements under a steady-state CO + NO reaction at the total pressure of 1×10^{-7} Torr of the equi-molar mixture of NO and CO in the range of 400–800 K. The ratio of $\{2[N_2]+[N_2O]\}/[CO_2]$ was confirmed to be kept at unity throughout the studied T_S, where $[N_2]$, $[N_2O]$ and $[CO_2]$ are the amount of each species estimated from their AI signals, i.e., only the reaction $(NO + CO) \rightarrow (N_2 + N_2O + CO_2)$ takes place [14].

The AR N_2 signals at $\theta = 0°$ and 41° are displayed in figure 2b, c because these are the collimation angles (the maximum flux position). The AR N_2O signal at $\theta = 0°$ is shown in figure 2d. The desorption of this species always showed a cosine distribution. There are noticeable differences in the temperature dependence of each component. At the pressure ratio of NO/CO = 1, the AR N_2 signal at 41° started to increase at 500 K, reaching quickly to the maximum at 530 K and then began to decrease above 550 K. On the other hand, the N_2 signal at $\theta = 0°$ increased slowly above 500 K and reached the maximum at around 600 K. This indicates remarkable shifts in the nitrogen removal pathway with increasing T_S. For the pressure ratio of NO/CO = 0.25, the N_2 signal at 41° remained invariant, whereas the signal at $\theta = 0°$ increased about twice, indicating that it was due to a different process. It should be noted that the AR N_2O signal at $\theta = 0°$ followed a T_S dependence similar to the N_2 at $\theta = 40°$ even for different NO/CO ratios, suggesting a common pathway. The overall reaction was reduced at the ratio NO/CO = 3 and showed two maximums. There was a critical CO pressure at which the product formation kinetics changed sharply (Figure 3a). This happened near the pressure ratio of NO/CO = 1 below 600 K, at which the NO reduction or the CO_2 formation was maximized, indicating that the surface was most deficient in O(a) [5]. The remarkable differences in the above T_S dependence of the AR N_2 signals between $\theta = 0°$ and 41° indicate drastic changes in the contribution of each N_2 desorption around the ratio of NO/CO = 1.

3.2. Desorption components

Desorbing N_2O showed the cosine distribution and its velocity distribution followed a Maxwellian distribution at the surface temperature, i.e., N_2O is once trapped on the surface before the desorption [14]. On the other hand, the angular distribution of desorbing N_2 largely depended on the surface temperature and CO/NO ratio. Below 550 K, the N_2 desorption sharply collimated at around 40° over a wide CO pressure range (figure 3a). The signal at the normal direction was less than 6% of that at 40°. At higher temperatures, however, the N_2 signal at the normal direction was enhanced, especially at high CO

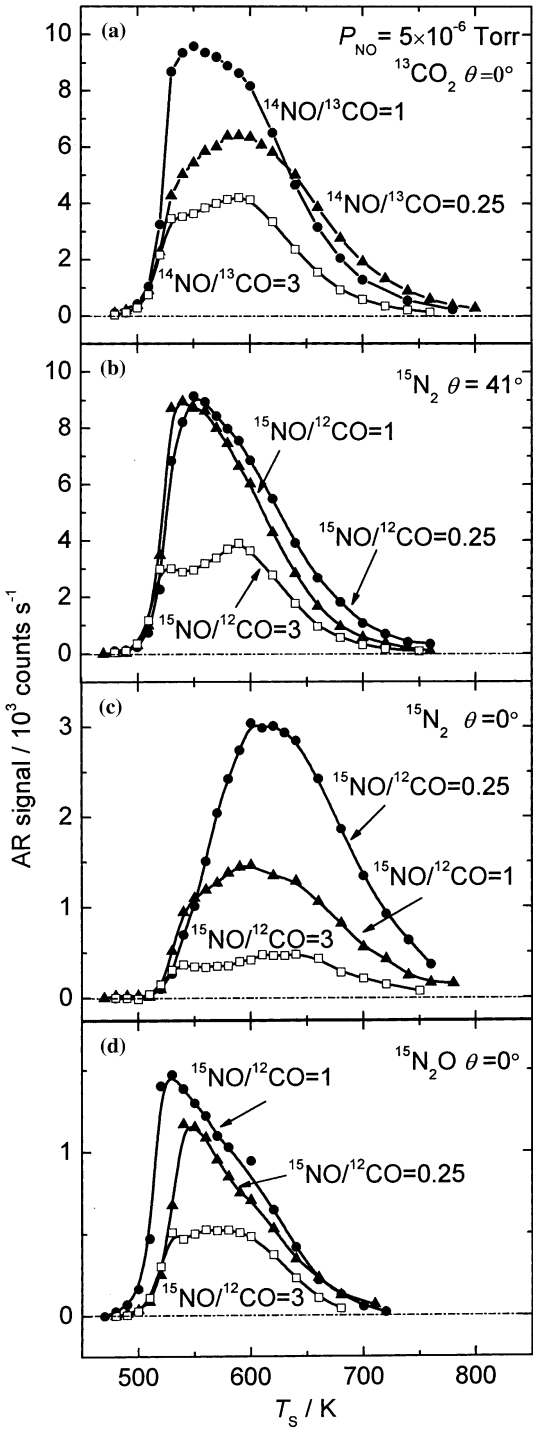

Figure 2. Surface temperature dependence of AR product signals at their collimation angles with different ^{15}NO + ^{12}CO(or ^{14}NO + ^{13}CO) mixtures at 5×10^{-6} Torr of ^{15}NO. (a) $^{13}CO_2$ at $\theta = 0$ °. It shows closely the overall reaction rate. (b) $^{15}N_2$ at $\theta = 41°$, (c) $^{15}N_2$ at $\theta = 0°$ and (d) $^{15}N_2O$ at $\theta = 0°$.

pressures as shown in figure 3b. The distribution was deconvoluted into three components based on the following velocity distribution analysis.

The velocity distribution curves of desorbing N_2 at different desorption angles at T_S = 640 K are shown in Figure 4. The apparent translational temperature calculated as $T_{<E>} =< E > /2k$ is shown in < > in the figure, where $< E >$ is the average kinetic energy and k is the Boltzmann constant. The value was maximized to 3230 K at around 40° and decreased quickly with an increasing shift from the collimation angle as expected from the inclined desorption. The velocity distribution involved the thermalized component as well as that faster than those expected by the Maxwell distribution at the surface temperature. The thermalized component follows a cosine distribution, and then it was first subtracted from the velocity distribution curves. The resultant velocity curve provided the flux of the fast component, which peaked at $\theta = 0°$ and 40°. The fast component yielded the maximum with the translational temperature of about 371 K at $\theta = 40°$, showing 2520 K at $\theta = 0°$. These values are shown in [ ] in the figure.

Assuming a power series of the cosine of the desorption angle shift from the collimation position to each component, the N_2 distribution was roughly in a two-directional form as $\{\cos^{28}(\theta+40) + \cos^{28}(\theta-40)\}$ and the signal at the normal direction was almost negligible below 600 K. With increasing T_S above 600 K, the normally directed component was enhanced. The total signal at 640 K was approximated as $0.71\ \{\cos^{28}(\theta+40) + \cos^{28}(\theta-40)\} + 0.19\ \cos^5\theta + 0.32\ \cos\theta$. The pre-factors indicate the relative intensity. The inclined N_2 desorption and the normally directed N_2 component showed different behavior toward the variation of the surface temperature and the pressures of CO and NO, indicating that they came from different nitrogen removal steps. The former was assigned to the decomposition of N_2O oriented along the [001] direction and the latter was due to the associative desorption of N(a) [7,8]. On the other hand, the cosine component cannot be assigned to a definite process from the angular distribution, i.e., the dynamic information has been lost. However, its kinetic behavior, i.e., its temperature dependence and CO and NO dependence, was similar to those of the normally directed N_2 desorption, suggesting the formation from the associative process. In fact, Ma recently found no thermalized N_2 component in a steady-state N_2O + CO reaction on Pd(110) in the range of 450–800 K, supporting this speculation [26].

3.3. *NO + CO + O_2 reaction*

The addition of oxygen changed the CO_2 and N_2 formation rates in different ways. The results at T_S = 550 K (NO/CO = 1 at $P_{NO} = 5 \times 10^{-6}$ Torr) are shown in Figure 5a, where the AI signals are displayed as a function of the oxygen pressure (P_{O2}). With increasing P_{O2}, the total CO_2 formation was once enhanced and then decreased, whereas both the N_2 and N_2O formation decreased monotonously. Similar results were observed at 640 K as well. The CO_2 increment is due to the enhanced supply of oxygen on the surface.

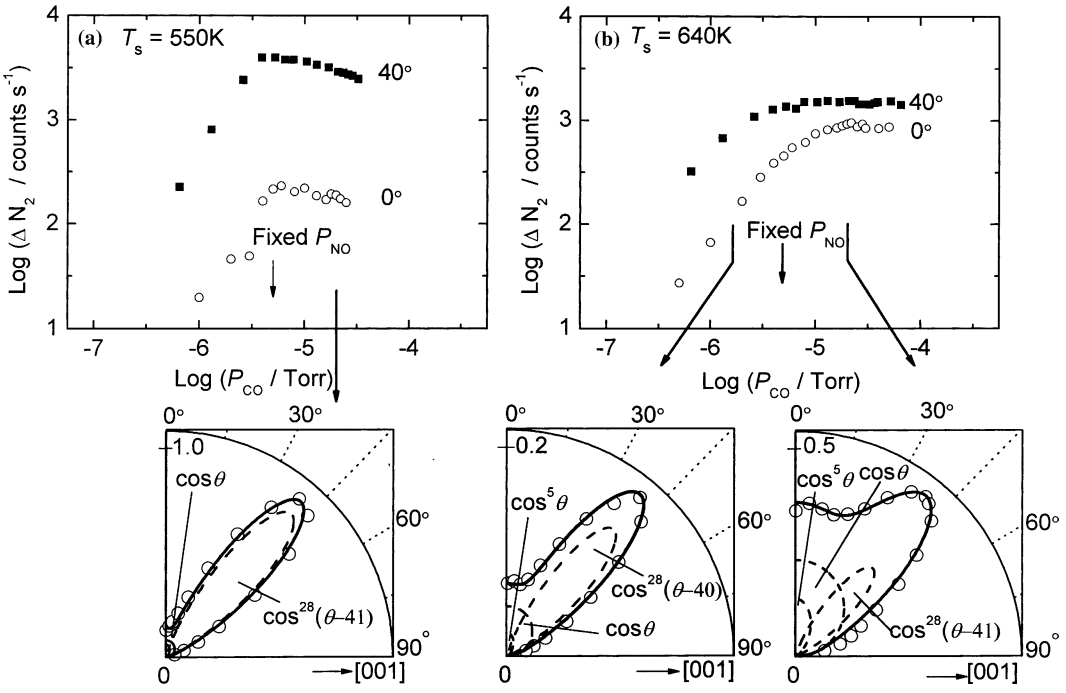

Figure 3. P_{CO} dependence of the AR $^{15}N_2$ signals at $\theta = 0°$ and 40° in the steady-state ^{15}NO + ^{12}CO reaction at 5×10^{-6} Torr of ^{15}NO and T_S = 640 K. The angular distributions of desorbing $^{15}N_2$ in the plane along the [001] direction are also shown at different CO pressures. Typical deconvolutions (see text) are drawn by broken curves. The ordinate was normalized to the maximum.

The contribution of the oxygen supply from NO to the CO_2 formation was estimated from the reaction stoichiometry as ($2[N_2] + [N_2O]$) and is shown by open symbols in the figure. It decreased quickly with increasing P_{O2} The NO dissociation was immediately retarded and completely suppressed above $P_{O2} = 2 \times 10^{-6}$ Torr.

AR-signal analysis illustrates the P_{O2} dependence of the branching ratio in more detail. At 550 K, the AR N_2 signal at $\theta = 40°$ decreased quickly with increasing P_{O2}, whereas the AR N_2O signal at $\theta = 0°$ decreased slowly. The branching ratio in the N_2O decomposition, i.e., the contribution ratio of process (ii) to process (i), was calculated after the total amount of the product in each process was estimated by taking account of the sharpness of the angular distribution and the AR signal intensity at the collimation position [16]. The branching ratio initially remained 0.25 and, above about 10% of the oxygen content, it increased steeply to 1.4 (figure 5b). This indicates that about 20% of the formed N_2O(a) was emitted without decomposition on the surface contacted with only an equi-molar (NO + CO) mixture, where the surface oxygen amount was minimized. In fact, the surface at this condition showed a (1 × 1) LEED pattern without any super structure. The fraction increased above 60% on oxygen-rich surfaces.

At 640 K, the branching was even worse than that at 550 K. The AR N_2 signal at $\theta = 40°$ decreased more quickly than the N_2O signal in a similar way to that at 550 K (figure 5c). The resultant branching is shown in the lower panel. It remained at around 0.30 and increased steeply at higher O_2 pressures. The value indicates that about 30% of the produced N_2O(a) was emitted without decomposition. At this high temperature, the normally directed N_2 desorption became significant. This component decreased most quickly with increasing P_{O2}. The branching ratio of N_2 formation in process (iii) to that in process (i) is shown after integration of the signals. It decreased from 0.46 to 0.27 with increasing P_{O2}. Here, process (iii) was treated to involve both the cosine and the normally directed $\cos^5\theta$ components. The former shares about 80% of the total formation in process (iii).

The angular and velocity distribution of CO_2 was almost insensitive to the oxygen pressure and quite close to those in the active region of the steady-state CO + O_2 reaction on Pd(110) [17].

4. Discussion

4.1. Inclined desorption mechanism

From AR-temperature-programmed desorption (TPD) work combined with TOF [11], the inclined N_2 desorption was first proposed to be due to the decomposition of N_2O oriented along the [001] direction. This orientation has already been confirmed by the density functional theory (DFT), near-edge X-ray absorption fine structure (NEXAS) and scanning tunneling microscopy (STM). DFT calculations at a Generalized

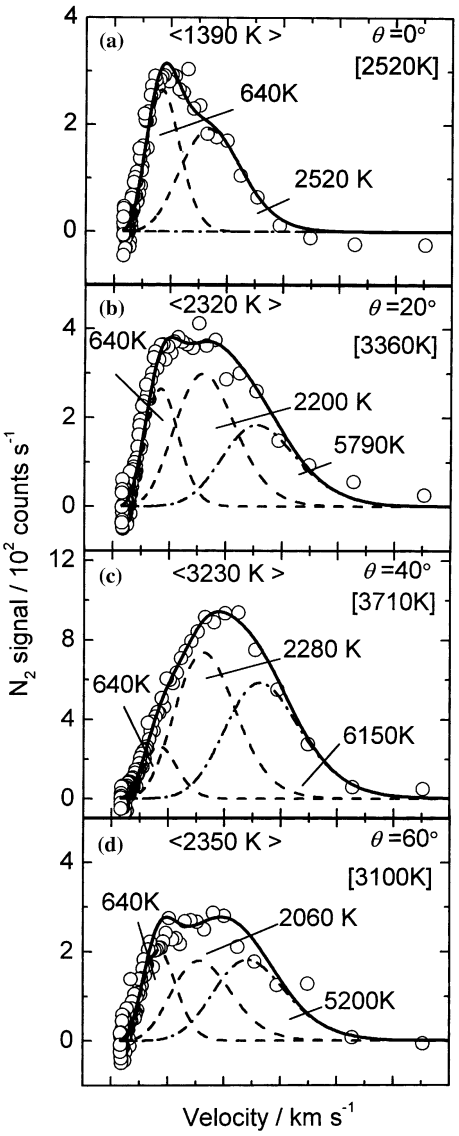

Figure 4. Velocity distributions of desorbing $^{15}N_2$ at different angles at T_S = 640 K and $^{15}NO/^{12}CO$ = 1/2 ($P_{NO} = 5 \times 10^{-6}$ Torr). The average kinetic energy and translational energy of fast components are indicated in < > and [ ] in temperature units, respectively. Typical deconvolutions (see text) are drawn by broken curves. The solid line indicates their summation.

Gradient Approximation level showed two stable adsorption forms, one lying along the [001] direction and another standing with the terminal nitrogen-metal bond [18,19]. No noticeable energy difference was found between them. In NEXAFS work at around 60 K, N_2O(a) showed two π resonance peaks at 401 and 405 eV of the photon energy. With increasing shift of the X-ray incident angle from the surface normal, their intensities increased significantly when the X-ray polarization was in a plane in the [001] direction, whereas for the polarization in the [110] direction, the intensities decreased. This anisotropy is explained by a mixture of the standing form and the lying along the [001] direction [20]. The STM observation was successful at 8 K after the clean surface was exposed to N_2O below 90 K [21]. N_2O formed clusters that extended to the [001] direction with a (1 × 1) periodicity, showing that N_2O was oriented along the [001] direction. The surface was in the (1 × 1) form even after N_2O adsorption.

A palladium (110) surface is reconstructed into a missing-row form after oxygen adsorption as designated by c(4 × 2)–O. This structure changes into the (1 × 1) without passing the meta-stable (1 × 2) form when the surface oxygen is removed above 355 K [22,23]. The observation of the (1 × 1) LEED pattern at the ratio of NO/CO = 1 suggests that the surface is deficient in O(a), being consistent with the maximized NO reduction rate. It is unlikely that the inclined N_2 desorption is due to the associative desorption of N(a) or the N_2O decomposition on the declined terrace of the c(4 × 2)–O structure. In the former, the collimation angle would be close to the local normal of the terrace, being shifted to a smaller value from the surface normal due to the surface smoothing effect [2]. In the latter, the N_2O decomposition must be suppressed by surface oxygen [24,25].

4.2. Branching mechanism

The AR N_2 signal at the normal direction was much less than that at 40° below 550 K. It means that only processes (i) and (ii) are operative. With increasing P_{CO} at 640 K, the signal at θ = 0° increased more rapidly than that at θ = 40°, showing that at around $P_{CO} = 1 \times 10^{-4}$ Torr, the integrated product from process (iii) overcame that of process (i). So the N_2O(a) desorption and decomposition was predominant at lower surface temperatures and higher NO pressure while the associative progress of N(a) was favored at higher surface temperatures and higher P_{CO}

In the steady state NO + CO + O_2 reaction on Pd(110), the angular and velocity distributions of the products were very similar to those in the NO + CO reaction, which suggests that the reaction pathways do not change by the addition of oxygen. The surface-nitrogen removal processes are likely to proceed on vacant areas outside oxygen-covered regions. The NO dissociation was retarded by the addition of O(a). The resultant reduced amount of N(a) decreased the surface-nitrogen removal processes in different ways. Generally, the branching of the N_2O decomposition is likely to be controlled by the amount of N(a), and the total NO reduction is controlled by the amount of O(a) and vacant sites. Process (iii), 2N(a) → N_2(g) is the most sensitive since it involves two nitrogen atoms, i.e., roughly speaking, a second-order reaction in N(a). Process (ii), NO(a) + N(a) → N_2O(a) → N_2O(g), is the most insensitive, since the N_2O(a) dissociation is also suppressed when the N_2O(a) formation is retarded by oxygen [24,25]. Eventually, process (i), NO(a) + N(a) → N_2O(a) → N_2(g) + O(a), becomes more sensitive. This is also consistent with the CO pressure dependence

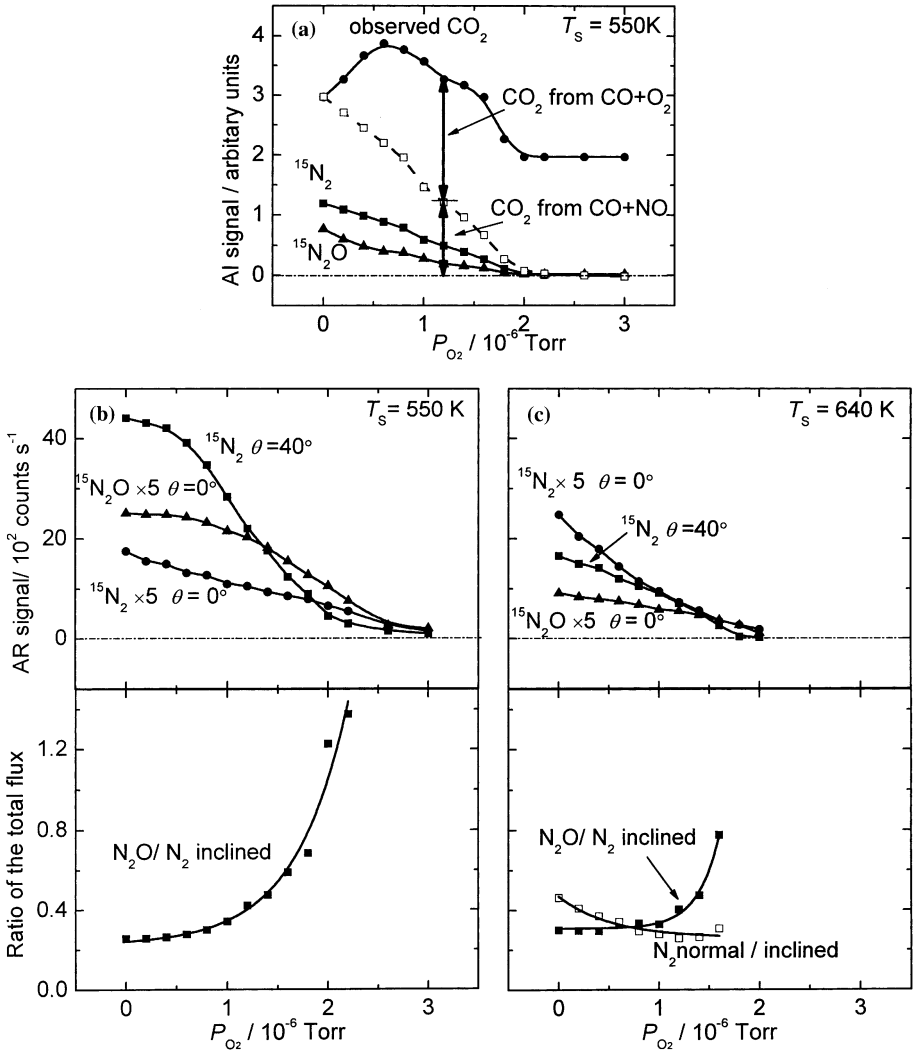

Figure 5. P_{O2} dependence of the product formation in the steady-state ^{15}NO + ^{12}CO ($^{15}NO/^{12}CO$ = 1) reaction at 1×10^{-5} Torr. (a) The AI signals at 550 K. The open symbols indicating the contribution from the NO dissociation were calculated from the stoichiometry. The AR $^{15}N_2$ signals at $\theta = 41°$ and 0° and the $^{15}N_2O$ at $\theta = 0°$ at T_S = (b) 550 K and (c) 640 K. The branching ratio of the $^{15}N_2O$ decomposition and the $^{15}N_2$ formation is shown in the lower panel. The normally directed desorption quantity in the ratio involves both the cosine and $\cos^5\theta$ components. The former shares 80% of the total quantity.

shown in figure 3, i.e., the normally directed desorption increased more rapidly than the inclined desorption along the enhanced overall reaction rate with increasing CO pressure.

4.3. Comparison with other surfaces

The oxygen effect on the NO + CO reaction has frequently been reported on Pd and Rh surfaces, but the surface-nitrogen removal processes have not been analyzed [12]. Graham *et al.* [27] studied the CO + O_2 and CO + NO reactions on Pd(100) by monitoring the total CO_2 signal under reaction conditions around several Torr. The rate for the reaction (CO + NO) was only about 2 orders of magnitude lower than that for (CO + O_2). The addition of O_2 increased the CO_2 formation rate below T_S = 500 K but had almost no effect on the rate of NO reduction. Permana [28] also reported that the CO_2 production rate was increased by a factor of ~4 by the addition of oxygen on Rh(111) with the reaction pressure of a few Torr. As was the case with the results on Pd(100), the formation rates of N-contained products (N_2 and N_2O) were insensitive to the presence of oxygen at lower P_{O2}. These were explained by the low oxygen coverage. However, Zaera *et al.* [12] showed that the addition of oxygen suppressed not only the NO reduction but also the CO oxidation on Rh(111) by using effusive molecular beams. The different behavior of the NO + CO reaction with oxygen was suggested to be due to different reaction mechanisms operative under UHV conditions and higher reaction pressures (~Torr).

No analysis of surface-nitrogen removal processes has been reported for a NO + CO reaction except for results at limited conditions on Pd(110) and Rh(110)

[14]. The mechanism involving the intermediate N_2O dissociation is more or less operative over different metals and various surface planes since this is a common byproduct over metal catalysts [29]. Its contribution must be sensitive to the reaction conditions. For example, N_2O(a) is easily formed from the reaction of NO(a) + N(a) on noble metals even below 200 K [2]. However, its conversion to N_2 is unlikely on fcc(111) such as Rh(111) [30], Ag(111) [31], Ni(111) [32], and Pt(111) [33] because N_2O(a) is desorbed without dissociation. On the other hand, below 200 K, N_2O(a) is easily dissociated on clean Rh(110), Pd(110) and Ir(110) [24,30,34], but its reactivity is sensitive to both the amount and the state of deposited surface oxygen [35–37]. The reactivity of fcc(100) is between (111) and (110) since its dissociation proceeds on Pt(100)(1 × 1) [38], and it is slow on Cu(100) and Ni(100) [39].

4.4. Dynamics and kinetics

By means of ordinary kinetic studies, it is difficult to evaluate the contribution of this N_2O intermediate dissociation process in the course of the catalyzed NO reduction because of the fast formation and decomposition of N_2O(a), the non-homogeneous reactivity of N(a) and the fast isotope exchange between N(a) atoms [40–42]. Infrared reflection absorption spectroscopy (IRAS) also fails to confirm this N_2O(a) intermediate, since the lying form is insensitive according to the dipole selection rule [43], and even the standing form is in excessively small amounts because of the small heat of adsorption [11.24]. Recently, the –NCO(a) intermediate was proposed from IRAS at higher pressures, but it was not observed below 2×10^{-2} Torr [44,45]. Furthermore, this –NCO(a) has not been confirmed to be related to the N_2 emission process [46]. The cooperative functions of different surface planes become important under real catalytic conditions when powdered metal catalysts are used on supporting materials.

This study demonstrates a few advantages of desorption dynamics over ordinary kinetic analysis when used for mechanism studies. Each surface elementary step involved in the catalytic processes can be studied in two ways, i.e., chemical kinetics and reaction dynamics. The first one treats the frequency (reaction rate) and the other handles the energy partition. The relaxation time of vibrationally excited molecules is in the order of 10^{-12} s on metal surfaces [47]. The molecule vibrates 10^2–10^3 times during this relaxation, and then the nascent fragment is likely to maintain high energy even after desorption. However, in thermally excited dissociation, the desorbed fragments have been believed to be trapped by (attractive) dispersion forces exerted from the surface unless they are repulsively desorbed. The collimated desorption from metal surfaces so far reported is limited to several associative desorption, such as CO(a) + O(a) → CO_2(g) and N(a) + N(a) → N_2(g). The product molecule is usually bulky and likely to be repelled by the surface at the moment of formation [2]. Thus, the N_2 emission from N_2O on Pd(110) is the first example to show collimated fragment desorption in thermal decomposition reactions. The reaction of NO + CO provides two kinds of characteristic N_2 desorption. Desorbing N_2 molecules are likely to be excited in the vibrational and rotational states as well [48,49]. The energy transfer mechanism can be examined from the internal energy distribution measurements such as resonance-enhanced multi-photon ionization (REMPI). In order to perform REMPI work, the product formation was mostly induced by dosing pulsed nitrogen atoms or ammonia beams to get sufficient density of desorbing nitrogen molecules, which were far from catalytic reaction conditions [50]. On the other hand, this NO + CO on Pd(110) can emit collimated N_2 beams with a constant flux. Thus, this will be a leading prototype reaction in the near future, though the CO oxidation has received much attention.

5. Summary

The branching of the intermediate N_2O(a) decomposition was studied in a steady-state NO + CO + O_2 reaction on Pd(110). With increasing supply of surface oxygen, the NO reduction was suppressed and the nitrogen-containing products decreased monotonously. Depositing surface oxygen retarded the surface processes in the sequence of the NO dissociation ≈ the N(a) combination > N_2O decomposition > N_2O formation. Then, the N_2O fraction increased in nitrogen-containing products at higher O_2 pressures. This sequence can be explained by the decreasing amount of surface nitrogen.

Acknowledgments

The authors thank Ms. Atsuko Hiratsuka for drawing figures. This work was partly supported by a 1996 Center-of-Excellence (COE) special equipment program of the Ministry of Education, Sports, and Culture of Japan.

References

[1] R. Burch and P.J. Millington, Catal. Today 26 (1995) 185.
[2] T. Matsushima, Surf. Sci. Rep. 52 (2003) 1.
[3] I. Kobal, A. Kokalj, H. Horino, Y. Ohno and T. Matsushima, Trends Chem. Phys. 10 (2002) 139.
[4] S. Matsumoto, Catal. Today 90 (2004) 183.
[5] V.P. Zhdanov and B. Kasemo, Surf. Sci. Rep. 29 (1997) 35.
[6] I. Kobal, I.I. Rzeznicka and T. Matsushima, in: *Recent Research Developments in Physical Chemistry*, Vol. 6 (Transworld Research Network, 2002) p. 391.
[7] T. Matsushima, Surf. Sci. 197 (1988) L287.
[8] M. Ikai and K.-I. Tanaka, J. Phys. Chem. B 103 (1999) 8277.
[9] J.I. Colonell, K.D. Gibson and S.J. Sibener, J. Chem. Phys. 104 (1996) 6822.
[10] M. Ikai and K.-I. Tanaka, Surf. Sci. 357–358 (1996) 781.

[11] Y. Ohno, K. Kimura, M. Bi and T. Matsushima, J. Chem. Phys. 110 (1999) 8221.
[12] C.S. Gopinath and F. Zaera, J. Catal. 200 (2001) 270.
[13] I. Rzeznicka, Md.G. Moula, L. Morales, Y. Ohno and T. Matsushima, J. Chem. Phys. 119 (2003) 9829.
[14] I.I. Rzeźnicka, Y.-S. Ma, G. Cao and T. Matsushima, J. Phys. Chem. B 108 (2004) 14232.
[15] Y.-S. Ma, I. Rzeznicka and T. Matsushima, Chem. Phys. Lett. 388 (2004) 201.
[16] G. Cao, Md.G. Moula, Y. Ohno and T. Matsushima, J. Phys. Chem. B 103 (1999) 3235.
[17] Md.G. Moula, S. Wako, G. Cao, K. Kimura, Y. Ohno, I. Kobal and T. Matsushima, Phys. Chem., Chem. Phys. 1 (1999) 3677.
[18] A. Kokalj, I. Kobal, H. Horino, Y. Ohno and T. Matsushima, Surf. Sci. 506 (2002) 196.
[19] A. Kokalj, I. Kobal and T. Matsushima, J. Phys. Chem. B 107 (2003) 2741.
[20] H. Horino, I. Rzeznicka, T. Matsushima, K. Takahashi and E. Nakamura, in: *UVSOR Activity Report 2002* (Institute for Molecular Science, Okazaki, Japan, 2003) p. 209.
[21] T. Matsushima, I. Rzeznicka, K. Watanabe, Y. Inokuchi, K. Ohshimo and N. Nishi, *Nano-technology Support Report 2004* (Institute for Molecular Science, Okazaki, 2004) 37.
[22] V.R. Dhank, G. Comelli, G. Paolucci, K.C. Prince and R. Rosei, Surf. Sci. 260 (1992) L24.
[23] I.I. Rzeznicka and T. Matsushima, Chem. Phys. Lett. 377 (2003) 279.
[24] H. Horino, S. Liu, A. Hiratsuka, Y. Ohno and T. Matsushima, Chem. Phys. Lett. 341 (2001) 419.
S. Liu, H. Horino, A. Kokalj, I. Rzeznicka, K. Imamura, Y.-S. Ma, I. Kobal, Y. Ohno, A. Hiratsuka and T. Matsushima, J. Phys. Chem. B 108 (2004) 3828.
[26] Y.S. Ma and T. Matsushima, J. Phys. Chem. B 109 (2005) in press.
[27] G.W. Graham, A.D. Logan and M. Shelef, J. Phys. Chem. 97 (1993) 5445.
[28] H. Permana, K.Y. Simon Ng, C.H.F. Peden, S.J. Schmieg, D.K. Lambert and D.N. Belton, Catal. Lett. 47 (1997) 5.
[29] V.I. Pârvulescu, P. Grange and B. Delmon, Catal. Today 46 (1998) 233.
[30] Y. Li and M. Bowker, Surf. Sci. 348 (1996) 67.
[31] L. Schwaner, W. Mahmood and J.M. White, Surf. Sci. 351 (1996) 228.
[32] P. Väterlein, T. Krause, M. Bässler, R. Fink, E. Umbach, J. Taborski, V. Wüstenhagen and W. Wurth, Phys. Rev. Lett. 76 (1996) 4749.
[33] N.R. Avery, Surf. Sci. 131 (1983) 501.
[34] H. Horino, I. Rzeznicka, A. Kokalj, I. Kobal, A. Hiratsuka, Y. Ohno and T. Matsushima, J. Vac. Sci. Technol. A 20 (2002) 1592.
[35] H. Horino, S. Liu, A. Hiratsuka, Y. Ohno and T. Matsushima, Chem. Phy. Lett. 341 (2001) 419.
[36] K. Imamura, H. Horino, I. Rzeznicka, A. Kokalj, I. Kobal, A. Hiratsuka, B.E. Nieuwenhuys and T. Matsushima, Surf. Sci. 566–568 (2004) 1076.
[37] K. Imamura and T. Matsushima, Catal. Lett. 97 (2004) 197.
[38] R. Sau and J.B. Hudson, J. Vac. Sci. Technol. 18 (1981) 607.
[39] H. Horino and T. Matsushima, J. Phys. Chem. B 109 (2005) in press.
[40] F. Zaera and C.S. Gopinath, J. Mol. Catal. A: Chem. 167 (2001) 23.
[41] F. Zaera and C.S. Gopinath, Chem. Phys. Lett. 332 (2000) 209.
[42] C.S. Gopinath and F. Zaera, J. Catal. 186 (1999) 387.
[43] N.V. Richardson and N. Sheppard, in: *Vibrational Spectroscopy of Molecules on Surfaces*, J.T. Yates Jr. and T.E. Madey (eds.), (Plenum Press, New York, 1987), p. 1.
[44] E. Ozensoy, C. Hess and D.W. Goodman, J. Am. Chem. Soc. 124 (2002) 8524.
[45] E. Ozensoy and D.W. Goodman, Phys. Chem., Chem. Phys. 6 (2004) 3765.
[46] Y. Ma and T. Matsushima, J. Phys. Chem. B. 109 (2005) in press.
[47] E.J. Heiweil, M.P. Casassa, R.R. Cavanagh and J.T. Stephensen, Ann. Rev. Phys. Chem. 40 (1989) 143.
[48] M.J. Murphy, J.F. Skelly and A. Hodgson, Chem. Phys. Lett. 279 (1998) 112.
[49] M.J. Murphy, J.F. Skelly and A. Hodgson, J. Chem. Phys. 109 (1998) 3619.
[50] A. Hodgson, Prog. Surf. Sci. 63 (2000) 1.